

# Supporting Information

## Broadband Tunable, Polarization-Selective and Directional Emission of (6,5) Carbon Nanotubes Coupled to Plasmonic Crystals

*Yuriy Zakharko<sup>\*,†</sup>, Arko Graf<sup>†,‡</sup>, Stefan P. Schießl<sup>†</sup>, Bernd Hähnlein<sup>§</sup>, Jörg Pezoldt<sup>§</sup>, Malte C. Gather<sup>‡</sup>, and Jana Zaumseil<sup>\*,†</sup>.*

<sup>†</sup> Institute for Physical Chemistry, Universität Heidelberg, D-69120 Heidelberg, Germany

<sup>‡</sup> SUPA, School of Physics and Astronomy, University of St Andrews, St Andrews KY16 9SS, United Kingdom

<sup>§</sup> Institut für Mikro- und Nanotechnologie, Technische Universität Ilmenau, 98693 Ilmenau, Germany

### Corresponding Authors

\* E-mail: yuriy.zakharko@pci.uni-heidelberg.de.

\* E-mail: zaumseil@uni-heidelberg.de.

## **1. Methods**

Sample fabrication and characterization

## **2. Results**

**A.** SEM images

**B.** 3D Finite-difference time-domain calculations

**C.** SWNTs photoluminescence lifetime

**D.** Reflectivity measurements of samples with 670, 830 and 1000 nm pitches

**E.** Angle-resolved photoluminescence of bare plasmonic crystals

**F.** SLR quality comparison for  $50 \times 50 \mu\text{m}^2$  arrays

**G.** Reliability test of the effect with a DPPT-BT polymer instead of SWNTs

## 1. Methods

**SWNTs dispersion preparation.** (6,5) SWNTs were prepared from CoMoCAT<sup>®</sup> raw material (diameter 0.7–0.9 nm, >93 % semiconducting SWNT, 773735 Sigma Aldrich, Lot #14J017A1). Poly[(9,9-dioctyluorenyl-2,7-diyl)-*alt-co*-(6,6'-2,2'-bipyridine)] (PFO-Bpy, American Dye Source, Mw = 34 kg/mol) was dissolved in toluene (2 g/L) before adding 1.5 g/L CoMoCAT and applying sonication using a bath sonicator for 50 min. During treatment with the ultrasonic bath (Bandelin Sonorex Digitec DT 102 H) the temperature was kept between 15 °C and 25 °C. Sonication was followed by centrifugation at 60,000 g (Beckman Coulter Avanti J26XP centrifuge) for 1 h. The supernatant was collected and the pelleted material was reused for repetitive dispersion with fresh polymer. (6,5) SWNTs were enriched by pelletizing the monochiral dispersion by ultracentrifugation (Beckman Coulter OptimaMax XP table-top) at 284,600 g for 20 h. The resulting pellet was redispersed in a small volume of toluene.

**Periodic arrays fabrication.** Electron-beam lithography (EBL) was performed on glass (Schott AF32 Eco) with a Raith 150 system (Raith GmbH). To avoid charging and to allow charge transport from back-scattered electrons, a 2 nm chromium layer was applied via physical vapor deposition (PVD) on top of the glass substrate. Subsequently a two-layer resist consisting of PMMA AllResist AR-P 617.03 (90 nm) and AR-P 679.02 (70 nm) was spincoated. The use of a two-layer resist enables an undercut, which is controlled by the annealing temperature (200 °C / 10 min for the AR-P 617.03 and 150 °C / 3 min for the AR-P 679.02). An additional 3 nm gold layer was sputtered on top to avoid charging. EBL was done by exposure in two steps with 10 kV and 60 μm aperture. The first step includes the fabrication of alignment markers on which, in the second step, the focus plane is adjusted, which enables exposure of larger structures in

contrast to focusing on the gold surface. After each of the two EBL steps 25 nm gold were applied using PVD. To enhance the adhesive strength the sample was sputtered with argon for 30 s at 100 W before metal deposition. The lift-off process was carried out using dimethylsulphoxide. The structures were oxidized in a rapid thermal annealing process at 500 °C for 30 s. The chromium layer was fully oxidized and had no impact on the plasmonic structure.

After a single drop casting (10  $\mu$ l) of the highly concentrated toluene dispersion of SWNTs samples were finalized by spincoating of a toluene solution (20 g/L) of poly(methyl methacrylate) (PMMA,  $M_w = 350000$ , Sigma Aldrich) at 1000 rpm. The same parameters were used to spincoat the PMMA layer on top of the bare plasmonic crystals.

For the additional test sample a 30 nm layer of the semiconducting near-infrared emitting copolymer DPPT-BT (poly(2,5-bis(2-octyldodecyl)-3,6-di(thiophen-2-yl)diketopyrrolo[3,4-*c*] pyrrole-1,4-dione-*alt*-benzo[*c*][1,2,5]thiadiazole),  $M_n=33$  kg/mol,  $M_w=87$  kg/mol, Flexink Ltd.) was spincoated at 2000 rpm for 60 s from a 8 g/L chlorobenzene solution, annealed at 200 °C for 30 min and covered with PMMA as stated above.

**Structural characterization.** The surface morphology of SWNTs films was characterized by atomic force microscopy (AFM, Bruker Dimension Icon) in tapping mode.

**Optical characterization.** The UV-Vis absorption spectrum of SWNTs layer was acquired with a Varian Cary 6000i absorption spectrometer. The photoluminescence excitation map was obtained by exciting the SWNT film with a wavelength tunable (1 nm step with laser-line tunable filter, Fianium Ltd.) output of a supercontinuum laser source (WhiteLase SC400, Fianium Ltd.) and detecting with an Acton SpectraPro SP2358 spectrometer (grating 150 lines/mm) and a liquid nitrogen cooled InGaAs line camera (PI Acton OMA V:1024 1.7).

The obtained signal was wavelength calibrated for sensitivity of the detection system and incident laser power (measured with a calibrated silicon photodiode power sensor).

**PL lifetime measurements.** Samples were illuminated through the substrate glass with wavelength-filtered at 580 nm (laser-line tunable filter, Fianium Ltd.), pulsed ( $< 10$  ps, 10 MHz) output of a supercontinuum laser source (WhiteLase SC400, Fianium Ltd.) focused with a  $100\times$  near-IR 0.8 N.A. objective. Emitted photons were collected with the same objective and spectrally dispersed with an Acton SpectraPro SP2358 monochromator coupled to an InGaAs/InP single-photon avalanche diode (Micro Photon Devices, Italy). Statistics of the arrival times of the photons were acquired with time-correlated single-photon counting module (PicoHarp 300, Picoquant GmbH) at time bin 4 ps. The instrument response function was estimated by tuning the laser filter to 980 nm and measuring the scattered light.

**PL Quantum Yield.** For PL quantum yield (QY) measurements a 580 nm laser beam was directed through the entrance port of an integrating sphere (LabSphere, Spectralon coating). The solid sample was mounted in the center of the sphere. Quantum yield measurements were performed according to de Mello *et al.*<sup>1</sup> The scattered laser light and PL signal were fiber-coupled to the Acton SpectraPro SP2358 spectrometer. Emission spectra were compared to PL spectra measured outside the sphere to account for re-absorption/re-emission effects in the integrating sphere.<sup>2</sup> All spectra were corrected for the spectral response of the systems with a calibrated tungsten halogen lamp.

## 2. Results

### A. SEM images

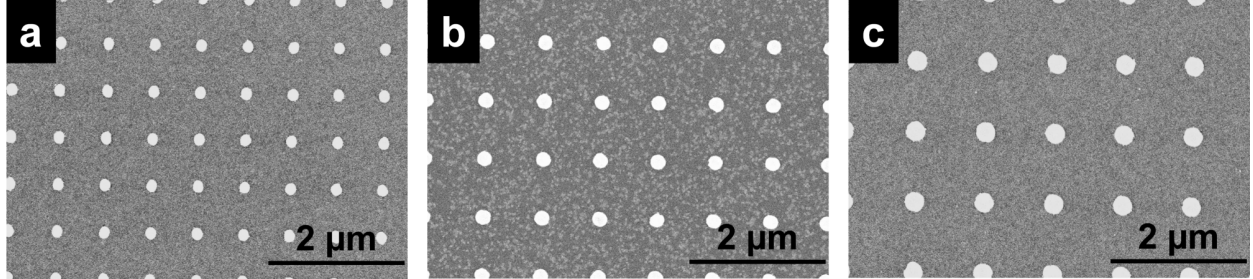


**Figure S1.** (a)-(c) Scanning electron micrographs of periodic arrays of gold nanodisks with 670, 830 and 1000 nm pitch and diameters  $D=160-180, 220$  and  $280$  nm, respectively.

### B. 3D Finite-difference time-domain calculations

3D finite-difference time-domain (FDTD) simulations were performed using commercial software (FDTD Solution v8.15.697, Lumerical Solutions Inc., Canada). A uniform mesh size of 6 nm (X, Y and Z-directions) was used in the region with a steep variation of the dielectric function ( $X \times Y \times Z = 670/(830/1000) \times 25 \times 670/(830/1000)$  nm<sup>3</sup> around gold nanodisk). Outside of these regions the grid was defined by the auto non-uniform mesh technique. The optical constants of gold and silver were taken from Johnson and Christy.<sup>5</sup> For TiO<sub>2</sub> refractive index was set to a constant value of  $n=2.48$ . The complex dielectric constant of the (6,5) SWNTs was represented by Lorentz model (Figure S2a) by fitting resonance frequency ( $\omega_0=1.88 \times 10^{15}$  rad/s), linewidth ( $\gamma=2.5 \times 10^{13}$  rad/s) and Lorentz permittivity ( $\epsilon_{\text{lorentz}}=0.04$ ) to the experimental absorbance spectrum (Figure 1d of the main text):

$$\epsilon(\omega) = \epsilon_r + \frac{\epsilon_{\text{lorentz}} \cdot \omega_0^2}{(\omega_0^2 - \omega^2) - 2i\gamma} \quad (2)$$

, with permittivity  $\epsilon_r=2.45$ .

An anisotropy in the Y-direction was added ( $n_y=1.56$  and  $k_y=0$ ) to take into account the in-plane (X-Z) orientation of the SWNTs.

The schematic layout of the simulation region (boundaries defined by periodic conditions and perfectly matched layers) is depicted in Figure S2b,c, including the glass substrate, a thin 100 nm SWNTs (or PMMA, with  $n=1.5$ ) layer covering gold nanodisks ( $h=20$  nm,  $D=180/220/280$  nm) and 150 nm of PMMA with  $n=1.5$ . To reduce computational resources and computational time, we took advantage of the symmetric/antisymmetric boundary conditions when possible. A TE or TM polarized plane wave was launched at different angles of incidence ( $0-50^\circ$ ) to the substrate, to calculate wavelength and angle dependent reflectivity (recorder by the top power monitor, dashed red line in Figure S2c). The minimum necessary thickness of top dielectric layer (i.e. 150 nm) was evaluated by varying the thickness of the layer in range of 0 to 240 nm (without SWNTs film) for the normal direction plane wave and calculating absorption of the nanodisks. As shown in the corresponding dependence in Figure S2d, 200-240 nm layer is sufficient to achieve strong SLRs response, while for the sample without top layer SLRs are not pronounced. These results lead to the value of 150 nm top PMMA layer above the 100 nm SWNTs film.

In order to estimate volume-averaged field intensity enhancement or field profiles we recorded electromagnetic fields with a 3D monitor (a uniform mesh size of 3 nm (X, Y and Z-directions)  $X \times Y \times Z = 670(/830/1000) \times 100 \times 670(/830/1000)$  nm<sup>3</sup>, red dashed line enclosing SWNTs layer in Figure S2b,c) or with 2D profiles monitor (a uniform mesh size of 2 nm, red dashed lines in Figure S2b,c). Field intensity enhancement  $|E_z/E_0|^2$  was calculated for plane wave injected normal to the surface (Z-polarized) by averaging values from the 3D monitor excluding values of cells/positions not representing SWNTs and dividing by the values of the structure without

gold/silver/TiO<sub>2</sub> nanodisk. For single (i.e. nonperiodic) gold nanodisk calculations the simulation region was extended to 3×3 μm<sup>2</sup> in X-Z-plane.

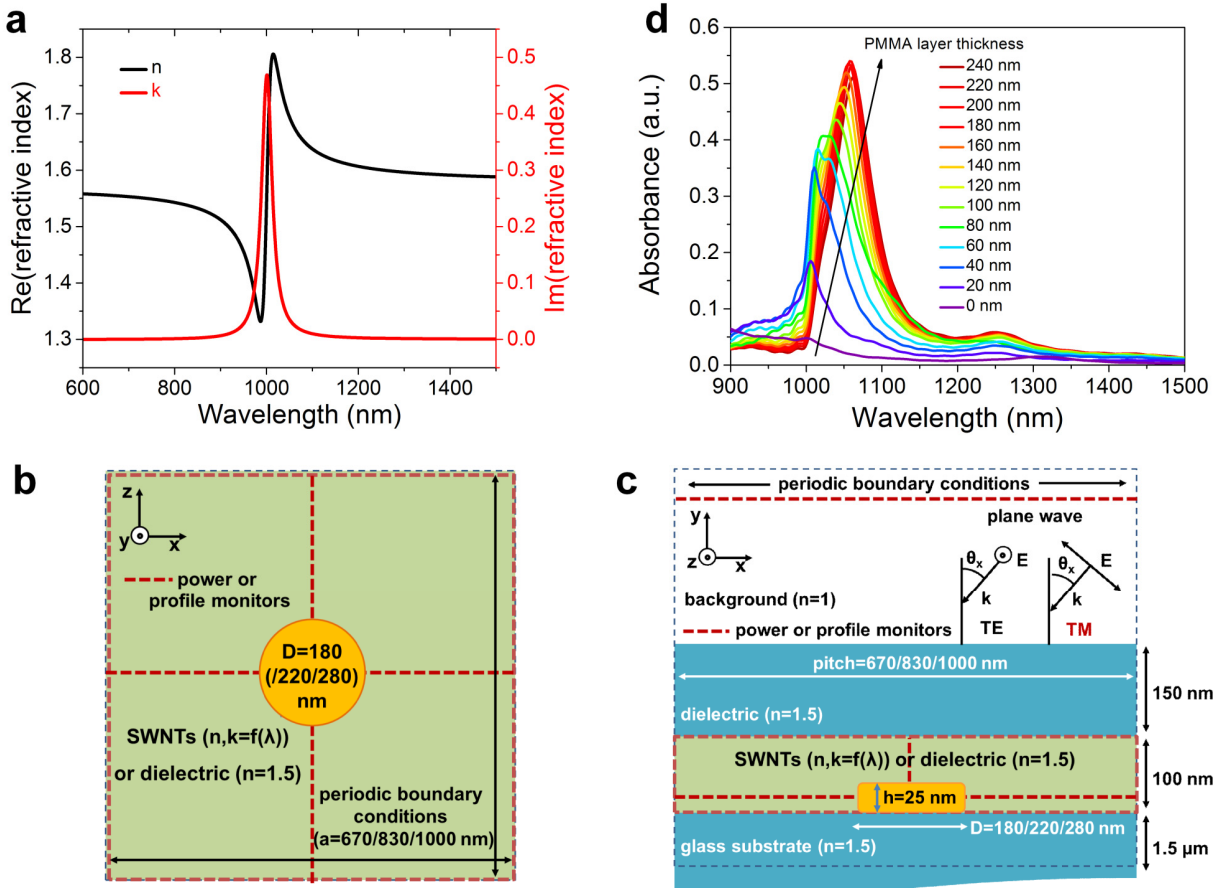


**Figure S2.** (a) Real and imaginary parts of complex refractive index of SWNTs networks layer. (b) and (c) Schematic layout of the 3D-FDTD calculations in X-Z and X-Y planes, respectively. Red dashed lines indicate power/field profile monitors. (d) Dependence of absorption of the gold nanodisks as a function of the top PMMA layer thickness (0-240 nm) without SWNTs layer.



### C. Photoluminescence lifetime

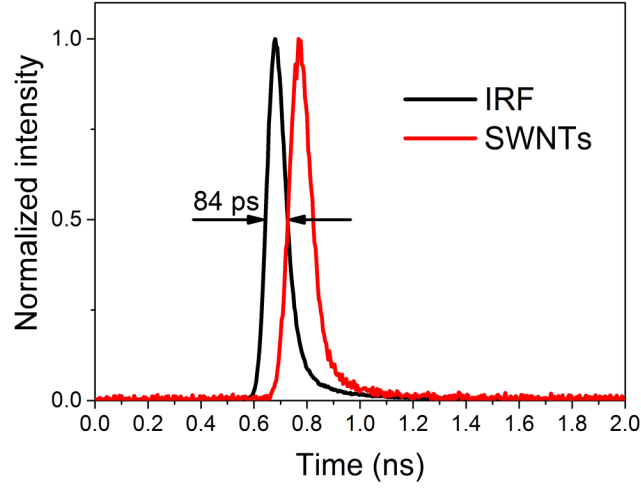


**Figure S3.** Photoluminescence decays for scattered laser (black line, detection/excitation at 980 nm) and (6,5) SWNTs (excitation 580 nm and detection 1005 nm) showing the same full width at half maximum.

The measured instrument response function (IRF) of the setup has the same full width at half maximum as the signal for SWNTs (Figure S3). Therefore, we conclude that the real PL lifetime is smaller than the theoretical limit of the reconvolution procedure of  $1/10^{\text{th}}$  of IRF, i.e.  $<8$  ps. This value is in good agreement with the expected lifetime, taking into account the radiative lifetime of excitons in SWNTs (1-10 ns)<sup>3,4</sup> and measured the PL quantum yield (0.1 %) defined as:

$$QY = 0.001 = \frac{1/\tau_r}{1/\tau_m} = \frac{\tau_m}{\tau_r} \Rightarrow \tau_m = \tau_r QY = 0.001 \cdot 1 - 10 \text{ ns} = 1 - 10 \text{ ps} \quad (1)$$

, where  $\tau_r$  and  $\tau_m$  are radiative and measurable lifetimes, respectively.

## D. Reflectivity measurements of samples with 670, 830 and 1000 nm pitches

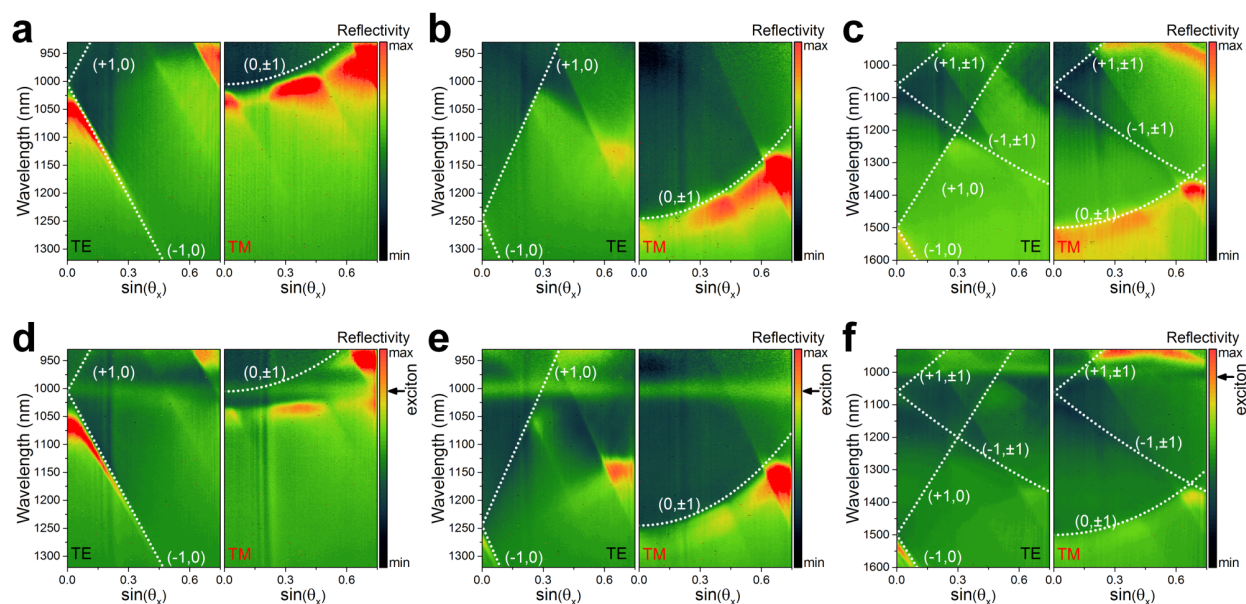


**Figure S4.** Angle-/polarization-dependent reflectivity spectra of samples with pitch 670, 830 and 1000 nm without (a)-(c) and with SWNTs (d)-(f), respectively. Analytical dependencies for corresponding Rayleigh anomalies are indicated with white dotted lines.

## E. Angle-dependent photoluminescence of bare plasmonic crystals

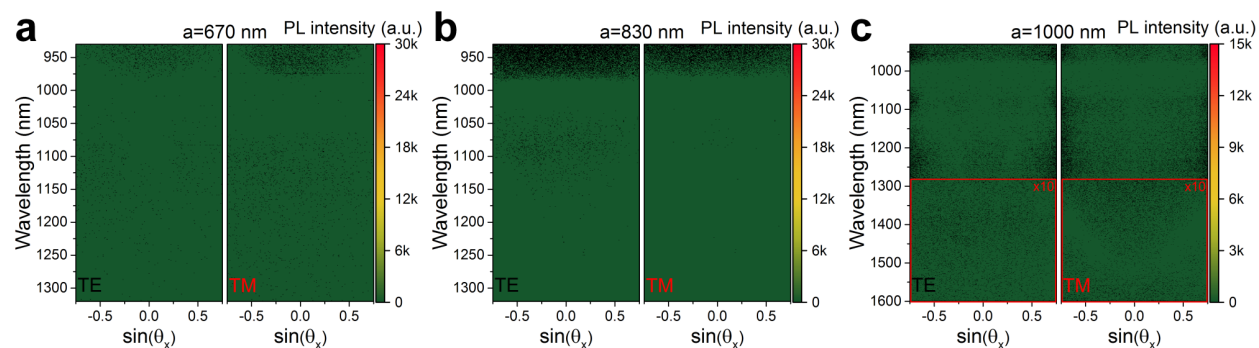


**Figure S5.** (a)-(c) Angle-/polarization-dependent photoluminescence spectra of bare (with PMMA but without SWNTs) plasmonic crystals with pitch 670, 830 and 1000 nm, respectively. Intensity scales are the same as in corresponding figures in the main text (i.e. Figure 3a-c).

## F. SLR quality comparison for $50 \times 50 \mu\text{m}^2$ arrays

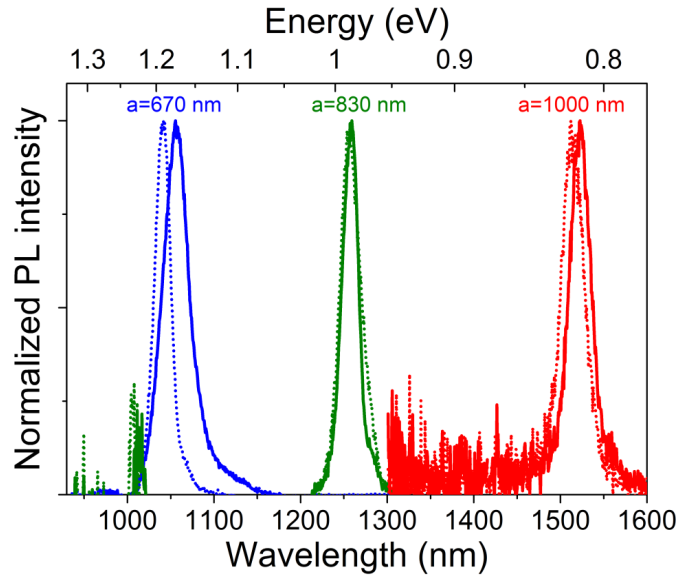


**Figure S6.** Comparative plot of normalized photoluminescence detected at normal incidence for samples with pitch 670 (blue line), 830 (green line) and 1000 nm (red line) with  $50 \times 50$  (dotted line) and  $100 \times 100 \mu\text{m}^2$  (solid line) periodic nanodisks arrays.

## G. Reliability test of the effect with a near-infrared emitting polymer instead of SWNTs

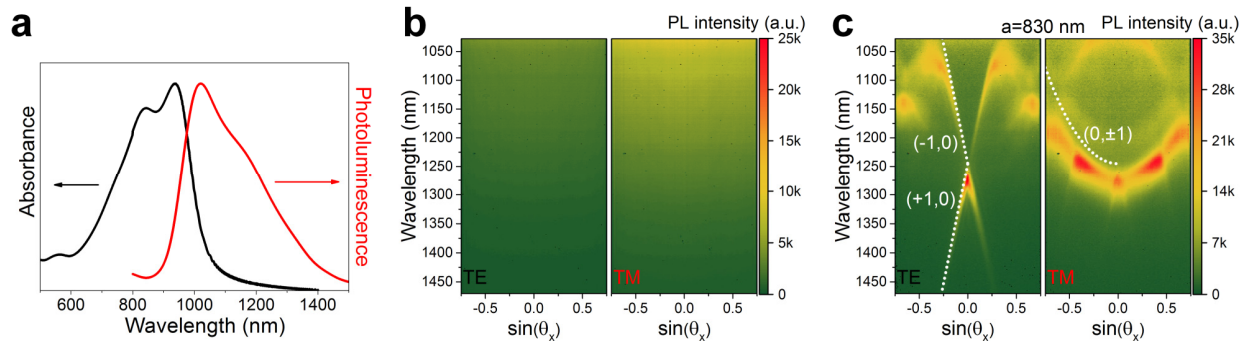


**Figure S7.** (a) Absorption and photoluminescence spectrum of a thin film of the near-infrared emitting polymer DPPT-BT. Angle-/polarization-dependent photo-luminescence spectra of the polymer layer without (b) and with (c) plasmonic crystals (830 nm pitch).

## REFERENCES

- (1) Mello, J. C. de; Wittmann, H. F.; Friend, R. H. *Adv. Mater.* **1997**, *9*, 230–232.
- (2) Ahn, T.; Al-Kaysi, R. O.; Müller, A. M.; Wentz, K. M.; Bardeen, C. J. *Rev. Sci. Instrum.* **2007**, *78*, 086105.
- (3) Spataru, C. D.; Ismail-Beigi, S.; Capaz, R.; Louie, S. *Phys. Rev. Lett.* **2005**, *95*, 247402.
- (4) Perebeinos, V.; Tersoff, J.; Avouris, P. *Nano Lett.* **2005**, *5*, 2495–2499.
- (5) Johnson, P. B.; Christy, R. W. *Phys. Rev. B* **1972**, *6*, 4370–4379.